CrossMark

Synthesis and characterization of a novel core–shell magnetic nanocomposite via surface-initiated RAFT polymerization for highly efficient and selective adsorption of uranium(VI)

Zhongran Dai[1] · Hui Zhang[1] · Yang Sui[2] · Dexin Ding[1] · Nan Hu[1] · Le Li[1] · Yongdong Wang[1]

Abstract

In this work, the nanoparticles possessing a macro-initiator (MNPs@SCSOEt) were firstly obtained by surface-initiated RAFT polymerization. The structure of the nanocomposite was characterized by FT-IR, SEM, TEM, TGA, XPS and VSM. The effects of pH, contact time, initial uranium concentrations, coexisting ions and temperature on the U(VI) adsorption by MNPs@PAO were investigated in detail. The adsorption process was found to be in good agreement with pseudo-second order kinetic model and Langmuir adsorption isotherm model. The maximum adsorption capacity was estimated to be 216.45 mg/g by fitting Langmuir model with the equilibrium data. The adsorption process was endothermic and spontaneous. In addition, the adsorption capacity of MNPs@PAO for U(VI) decreased slightly after five successive adsorption/desorption cycles.

Keywords Uranium(VI) · Magnetic nanocomposite · Surface-initiated RAFT polymerization · Adsorption

Introduction

Uranium, as one commonly used nuclear fuel for nuclear power, has played an important role in alleviating shortage of fossil fuels and slowing global warming. Simultaneously, uranium mining and processing have generated large amount of uranium-containing wastewaters [1–3]. These wastewaters have posed a serious threat to the environment and organism since the uranium in them is radioactive and toxic. Thus, it has been a research focus to develop effective techniques for removal of uranium(VI) from radioactive wastewaters so as to ensure the sustainable development of nuclear power.

In the past decades, many techniques including ion exchange, liquid–liquid extraction, co-precipitation and adsorption have been proposed for removal of uranium(VI) from wastewater [4–12]. Since adsorption has been found to be low in cost and high in adsorption capacity and generate no secondary contamination, it has been extensively utilized for the removal of uranium(VI) from radioactive wastewater. Until now, a variety of adsorbents such as magnetic materials, activated carbon, graphene oxide, polymers and other materials have been developed for adsorption of uranium(VI), and some of them have been found to have good performance [13–33]. Nevertheless, it is still a challenge to develop new adsorbents with high adsorption capacity and selectivity for uranium(VI).

Magnetic nanoparticles (MNPs) have attracted considerable attention due to their magnetic properties, nanoscale features, and the potential applications in areas such as drug delivery, magnetic resonance imaging, cell separation, and removal of heavy metal ions [34–36]. Many studies have shown that MNPs with a layer of a coating material can prevent agglomeration of the cores, improve stability, and facilitate further functionalization [37]. Therefore, developing a feasible method for surface engineering of MNPs is of crucial importance for improving adsorption capability effectively. In fact, many surface-functionalized MNPs have been reported to show good performance for adsorption of uranium(VI) from wastewater. For example,

✉ Dexin Ding
  dingdxzzz@163.com

1   Key Discipline Laboratory for National Defense for Biotechnology in Uranium Mining and Hydrometallurgy, University of South China, Hengyang 421001, China

2   Hunan Taohuajiang Nuclear Power Co., Ltd, Yiyang 413000, China

Sun et al. [38] reported a magnetic nanocomposite Fe_3O_4@ZIF-8 which could fast adsorb and separate UO_2^{2+} ions from aqueous solutions; Chen et al. [27] prepared a core–shell structured Fe_3O_4@PDA@PAO MNPs which showed remarkable adsorption capacity toward uranyl ions at pH 5.0.

Considering simple operation, environmental benign and low cost, polymers have become the popular adsorbents for adsorption of uranium(VI) from wastewater. Nowadays, several studies have focused on the modified polymeric fiber adsorbent, especially poly (acrylamidoxime)-functionalized fiber, which has been considered to be one of the most effective polymeric fibers for adsorbing uranium(VI) [39–43]. In order to take full advantage of the polymer for highly effective adsorption of uranium(VI), growing polymer brushes on the surface of nanomaterials using controlled/living polymerization techniques is an attractive approach that provides a new strategy for the surface modification or functionalization for nanomaterials. This allows the polymerization to be directly started from initiator-anchored surfaces with accurate control over composition and architecture [44]. Among the major controlled/living radical polymerization techniques, reversible addition-fragmentation chain transfer (RAFT) is one of the most promising of forming polymers with controlled architectures around nanoparticles. Overall, based on the above mentioned advantages of both MNPs and polymers, it is possible to get an efficient adsorbent for adsorbing uranium(VI) from solution by modifying the surface of MNPs using the method of surface-initiated RAFT polymerization.

Herein, we report a novel core–shell magnetic nanocomposite via surface-initiated RAFT polymerization for uranium(VI) adsorption. The synthesis strategy for this material was planned. The nanoparticles possessing a macro-initiator (MNPs@SCSOEt) were firstly obtained by modifing the surface of Fe_3O_4 core with tetraethyl orthosilicate (TEOS), aminopropyltriethoxysilane (APTES), 2-bromopropionyl bromide and ethyl potassium dithiocarbonate, respectively, the chains of polyacrylonitrile (PAN) were then grafted onto MNPs@SCSOEt by surface-initiated RAFT polymerization using AIBN as initiator, and the derived intermediate (MNPs@PAN) was finally functionalized with amidoxime (AO) and a novel core–shell magnetic nanocomposite (MNPs@PAO) was obtained. In this way, high density well-defined polyacrylonitrile chains were covalently grafted on the surface of aminosilica-coated iron oxide nanoparticles, and they were subsequently converted to AO-functionalized polymer. The adsorption behavior of uranium(VI) by MNPs@PAO was also investigated in detail. The objective of this research was to offer a novel strategy for synthesizing new high-performance materials with high adsorption capacity and selectivity for uranium(VI) in solution.

Experimental

Materials

Acrylonitrile (AN) was purchased from Acros and passed through an activated alumina column prior to use. 2-bromopropionyl bromide and ethyl potassium dithiocarbonate (KSCSOEt) were purchased from TCI (Shanghai) Development Co., Ltd. Azobis-(isobutyronitrile) (AIBN), Ethylsilicate (TEOS) and (3-aminopropyl) triethoxysilane (APTES) were purchased from Kermel Chemical Reagents Development Center (Tianjin, China).

The stock solutions of uranium(VI) (1.0 g/L) were prepared in the following procedure: 1.1792 g U_3O_8 powder was first dissolved in hydrochloric acid (10 mL), hydrogen peroxide (3 mL) and two drops of nitric acid by heating in the sand bath; and the mixture was then cooled to room temperature and diluted with ultrapure water to 1000 mL, which was the standard solution of uranium. The solutions with different uranium(VI) concentrations for experiments were prepared by diluting the stock solution using ultrapure water.

Characterizations

Fourier-transform infrared (FT-IR) spectra of the samples were measured by IR Prestige-21 using standard KBr pellets. The morphology of the synthetic products was characterized using scanning electron microscope (SEM, Zeiss Merlin microscope) and transmission electron microscopy (TEM, JEM-2010) with an accelerating voltage of 200 kV. Thermogravimetric analysis (TGA) of samples was carried out using a TA-60Ws with a heating rate of 10 °C/min from 25 to 800 °C in nitrogen atmosphere. The MPMS SQUID VSM (vibrating sample magnetometer) was applied to test magnetic properties through measuring the function between magnetization and applied-field from − 10 to 10 kOe at 300 K. X-ray photoelectron spectroscopy (XPS) of samples was measured by ESCALAB 250Xi.

Synthesis of MNPs@PAN

The mixture of MNPs@SCSOEt (200 mg), acrylonitrile (0.59 mL), toluene (1 mL), and AIBN (10 mg) was sonicated in a 50 mL flask under nitrogen gas protection until a homogeneous solution suspension was formed. Subsequently, the flask was immersed into an oil bath at 80 °C with magnetic stirring for 1 h. After cooling to room temperature, the solid was easily isolated by applying external magnetic field and washed with ethanol and deionized water for several times. The product was kept being dried in vacuum at 50 °C for 24 h.

Synthesis of MNPs@PAO

200 mg MNPs@PAN and 1 mL NH_2OH (50% in water) were dispersed into 40 mL methanol–water ($V_m/V_w = 1/1$) solution. The mixed suspension was kept being stirred at 80 °C for 12 h. After cooling to room temperature, the solid was isolated by applying external magnetic field and washed with ethanol and deionized water for several times. The product was kept being dried in vacuum at 50 °C for 24 h.

Adsorption behavior toward U(VI)

The effects of pH, contact time, initial uranium concentrations, coexisting ions and temperature on the U(VI) adsorption by MNPs@PAO were investigated in detail. Typically, 10 mg adsorbent was added to a U(VI) solution (20 mL) with appropriate concentration and appropriate pH value in a 50 mL plastic tube shaken in air bath oscillator at 150 rpm and appropriate temperature. The pH was adjusted by a negligible volume of dilute HNO_3 or NaOH. After the tube was shaken for predetermined time, the solid–liquid separation was conducted using a magnet. The concentration of U(VI) in the solution was analyzed by the Br-PADAP method with a Visible Spectrophotometer at 578 nm (National Standard of the People's Republic of China, EJ 267.4-1984). All the experiments were performed in duplicates and a blank sample was set at the same time to minimize experimental error.

The amount of U(VI) adsorbed on the adsorbent (q_e) and distribution coefficient K_d (mL/g) were calculated using the following formulas:

$$q_e = \frac{(C_O - C_e)V}{m} \tag{1}$$

$$K_d = \frac{C_0 - C_e}{C_e} \times \frac{1000V}{m} \tag{2}$$

where q_e is the equilibrium adsorption capacity (mg/g), C_o and C_e are the concentrations of U (VI) before and after adsorption (mg/L), respectively, V is the liquid phase volume (L), and m is the amount of adsorbent (g).

Desorption and regeneration studies

To evaluate the stability and reusability of MNPs@PAO material, the experiments were performed in five consecutive adsorption–desorption cycles. In each cycle, 10 mg adsorbent was added to a 20 mL uranium(VI) solution (100 mg/L) in a 50 mL plastic tube, and the tube was shaken on air bath oscillator at pH 6.0 and temperature 298.15 K for 8 h. After that, the sorbent was separated with a permanent magnet. Adsorbent loaded with uranium(VI) was eluted using 0.1 M HCl solution (20 mL) as elutant, and washed with large amount of ultrapure water. Then, it was reused for uranium adsorption as before until the fifth cycle was completed.

Results and discussion

Synthesis and characterization

The synthesis of core–shell magnetic nanoparticles (MNPs@PAO) by surface-initiated RAFT polymerization is illustrated in Scheme 1. MNPs@SCSOEt was synthesized according to a reported procedure [44, 45]. Figure 1 shows the FT-IR spectra of MNPs@SCSOEt, MNPs@PAN and MNPs@PAO. The characteristic peak of $C \equiv N$ stretching vibration at 2243 cm^{-1} can be observed in the spectrum of MNPs@PAN, which indicates that polyacrylonitrile was introduced onto the MNPs@SCSOEt by surface-initiated RAFT polymerization [46]. After hydroxylamine treatment, the peak at 2243 cm^{-1} related to $C \equiv N$ disappears and the new characteristic peaks for $-NH_2$ (or –OH), C=N and N–O appear at 3115, 1659 and 916 cm^{-1}, respectively, which indicates that the nitrile groups in MNPs@PAN were completely converted into the amidoxime group [47, 48].

The SEM and TEM images of Fe_3O_4, MNPs@SCSOEt, MNPs@PAN and MNPs@PAO are shown in Fig. 2. It is clear that the average diameter of MNPs was about 200 nm. The surface of MNPs@SCSOEt particles became smoother after they were modified with macro-initiator (Fig. 2b), and the macro-initiator layers grew around the Fe_3O_4 cores (Fig. 2f). While the surface initiated RAFT polymerization was taking place, the PAN polymer brushes were growing on the MNPs@SCSOEt nanoparticles, and the obvious PAN layers were growing around the MNPs@SCSOEt (Fig. 2c, g). Finally, the core–shell structure of MNPs@PAO from AO-functionalization was still maintained, as shown in Fig. 2h.

The TGA curves of Fe_3O_4, MNPs@SCSOEt and MNPs@PAO are shown in Fig. 3. The weight loss of Fe_3O_4 was 11.85%, which was probably due to the evaporation of moisture and solvents. As a comparison, the weight losses of MNPs@SCSOEt and MNPs@PAO were 27.99 and 65.14%, respectively, which indicates that the shell layer of organic on the surface of Fe_3O_4 decomposed. In particular, the MNPs@PAO sample had a remarkable weight loss at about 200 and 650 °C, which was probably attributed to the decomposition of the amidoxime group and the total decomposition of the polymerized amidoxime group, respectively [49, 50]. These results further proved that the MNPs@PAO adsorbent was successfully prepared.

Magnetic properties are important for the magnetic separation process. Therefore, the magnetic behavior of the
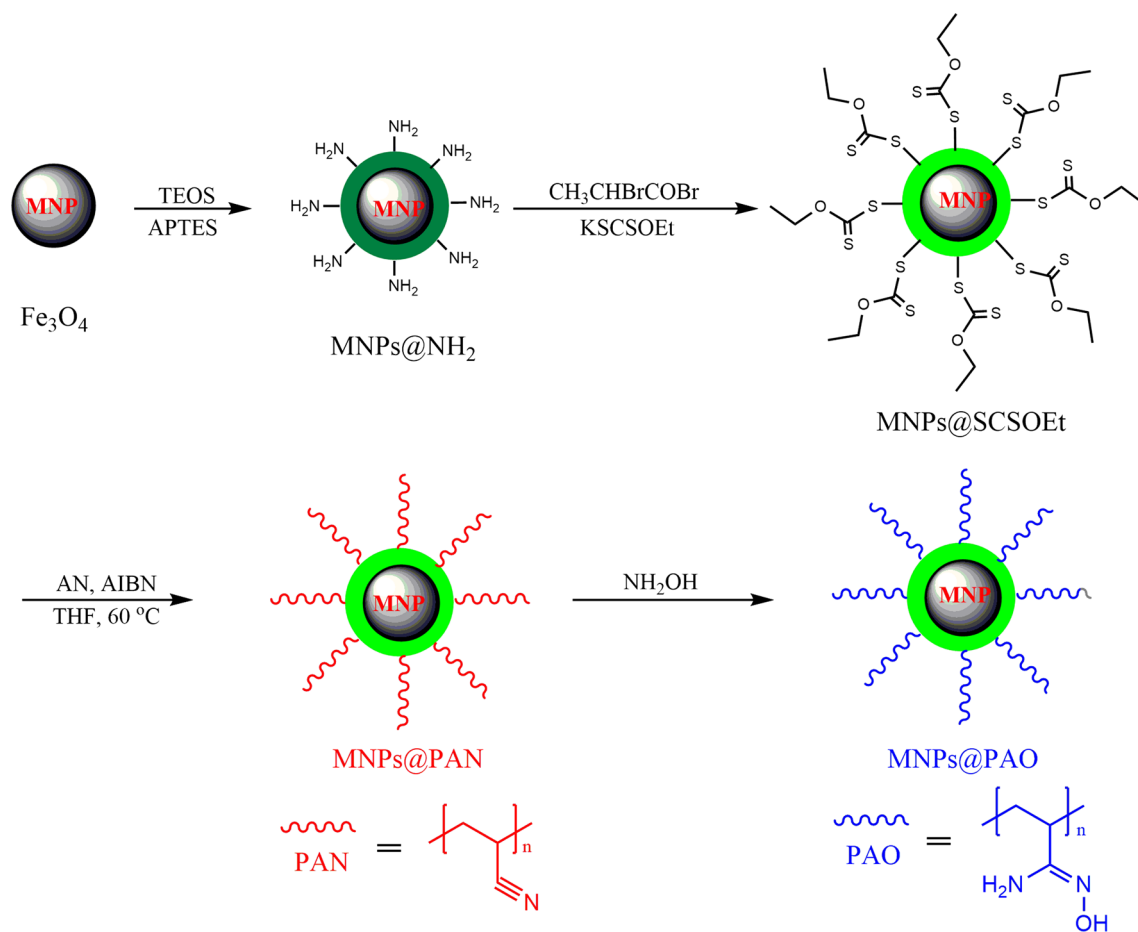
Scheme 1 Procedure for synthesizing the poly-amidoxime functionalized core–shell magnetic nanoparticles
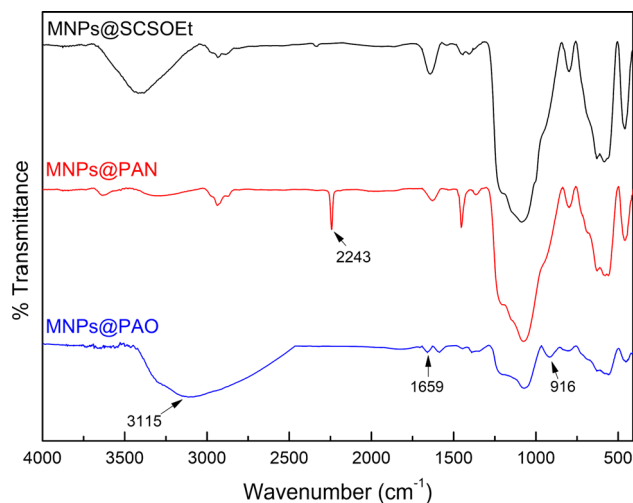

Fig. 1 FT-IR spectra of MNPs@SCSOEt, MNPs@PAN and MNPs@PAO

Fe_3O_4, MNPs@SCSOEt and MNPs@PAO was characterized by vibrational sample magnetometer (VSM). As shown in Fig. 4, the saturation magnetization values of Fe_3O_4 (64.93 emu/g), MNPs@SCSOEt (36.57 emu/g) and

MNPs@PAO (27.04 emu/g) were decreased in turn, which was due to the silica coating and the organic functional shell modifications. Nevertheless, no hysteresis loops were observed at VSM curve of MNPs@PAO and the remanence was negligible, which indicates that MNPs@PAO was still superparamagnetic at room temperature [51, 52]. In fact, the magnetic separation of MNPs@PAO particles was accomplished within 12 s in the adsorption experiment.

The chemical binding states on the surface of the samples were further investigated by XPS. As shown in Fig. 5, a new strong double U4f peak in the XPS spectrum of MNPs@PAO-U (uranium-loaded MNPs@PAO after adsorption), and the corresponding high-resolution $U4f_{5/2}$ and $U4f_{7/2}$ peaks at 392.28 and 381.48 eV, respectively, in its XPS spectrum appeared, which indicates that uranium existed in the MNPs@PAO-U sample after adsorption [53, 54]. The N1s spectra of the MNPs@PAO samples are shown in Fig. 6a, which shows that the N1s of MNPs@PAO consisted of the $H_2\underline{N}$–C=N–OH and H_2N–C=N–OH at 399.28 and 399.98 eV, respectively. By contrast, the N1s fitted with $H_2\underline{N}$–C=N–OH and H_2N–C=$\underline{N}$–
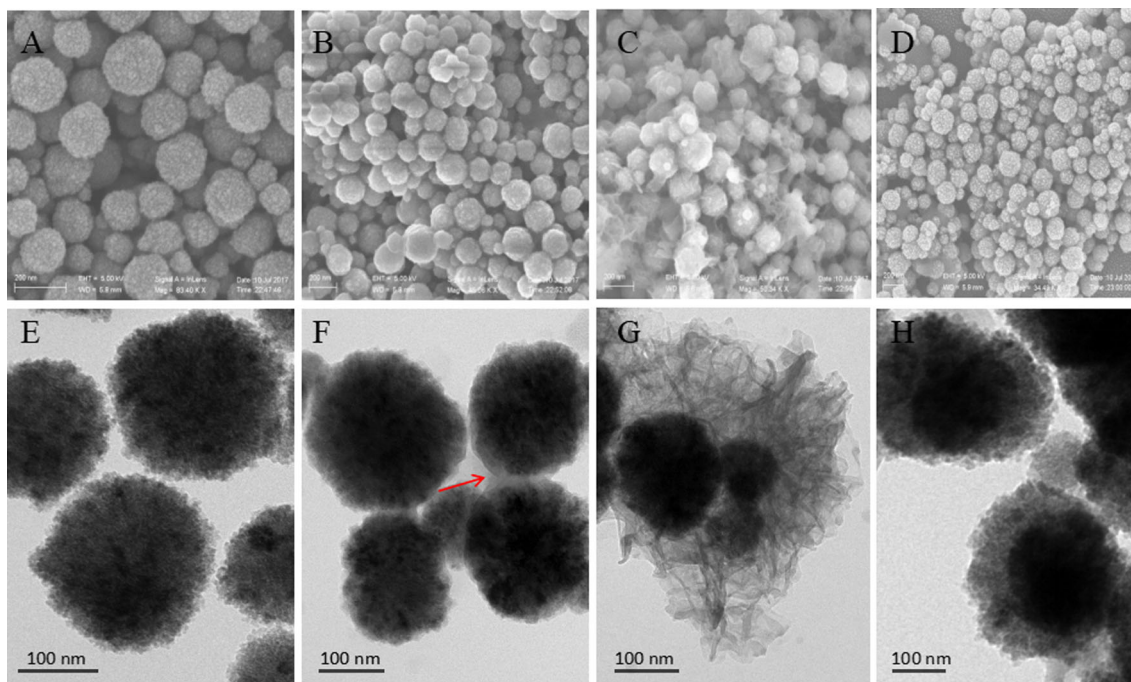
Fig. 2 SEM images of **a** Fe_3O_4, **b** MNPs@SCSOEt, **c** MNPs@PAN, and **d** MNPs@PAO and TEM images of **e** Fe_3O_4, **f** MNPs@SCSOEt, **g** MNPs@PAN, and **h** MNPs@PAO
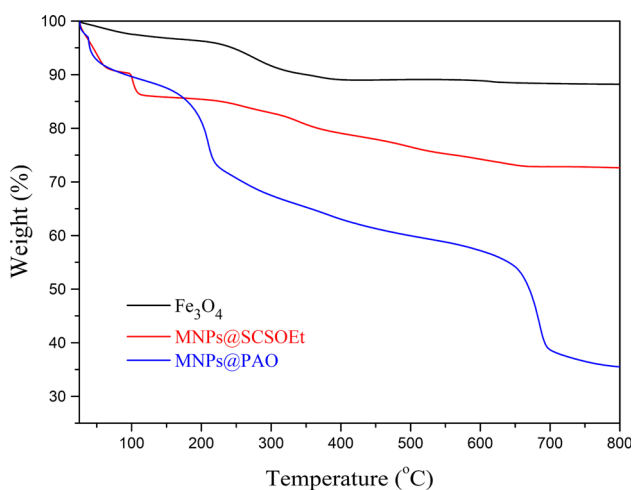

Fig. 3 TGA curves of Fe_3O_4, MNPs@SCSOEt and MNPs@PAO

Fig. 4 Magnetization curves of Fe_3O_4, MNPs@SCSOEt and MNPs@PAO

OH peaks at 399.38 and 401.08 eV, respectively, after MNPs@PAO was loaded with uranium (Fig. 6b). Meanwhile, the C1s of MNPs@PAO fitted with C–C/C–H, H_2N–C=N–OH, and C=O peaks at 284.78, 286.18, and 288.18 eV, respectively (Fig. 6c). After adsorption, the peaks consisting of C–C/C–H, H_2N–C=N–OH and C=O at 284.78, 286.48 and 288.48, respectively fitted well with the C1s curve of MNPs@PAO-U (Fig. 6d). In addition, the O1s of MNPs@PAO fitted with C=N–OH and adsorbed water peaks at 531.08 and 529.83 eV, respectively (Fig. 6e). After adsorption, the C=N–OH and adsorbed
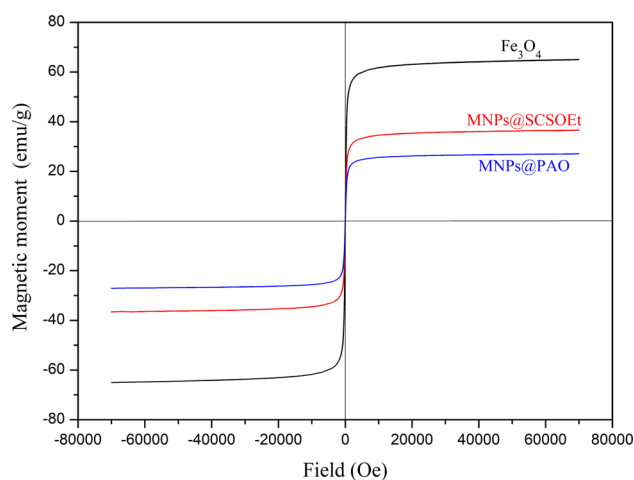
water peaks at 531.99 and 529.92, respectively (Fig. 6f). It is observed that the peaks for MNPs@PAO became wider and moved to higher binding energy after it was loaded with uranium, which is consistent with the result reported in literature [55, 56]. According to the XPS analysis, after the adsorption of uranium(VI), the binding energy of C=N–OH was shifted 0.91 eV to higher binding energy, indicating the coordination of uranium(VI) with oxime oxygen. In addition, the binding energy of C=N–OH also moved to higher binding energy after it was loaded with uranium(VI). Therefore, we believe that the MNPs@PAO
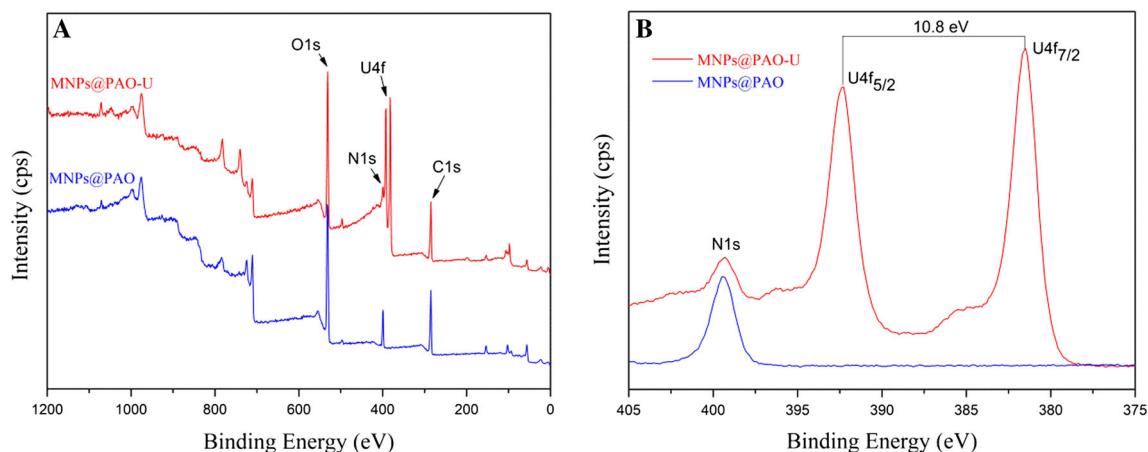
Fig. 5 XPS spectra of MNPs@PAO-U and MNPs@PAO

bind uranium(VI) through the $\eta 2$ mode [57, 58] which is the possible $\eta 2$ chelating mechanism, as shown in Fig. 7. The results of XPS analysis also provided evidences for the structure of MNPs@PAO and further demonstrated the successful preparation of MNPs@PAO.

Effect of solution pH

The pH of the solutions is an important factor for adsorption of metal ions. First, the effect of pH on uranium adsorption by MNPs@PAO from solutions with pH from 3 to 8 was investigated. As shown in Fig. 8, the U(VI) adsorption on MNPs@PAO depends strongly upon pH, and the maximum adsorption capacity could be reached at pH 6.0 (q_e = 165.8 mg/g). The results could illustrate the surface protonation reaction [27, 59]. In acidic conditions (pH < 6), the amino groups will be protonated, which prevents the chelating reaction between the amidoxime ligands and uranyl ions. Nevertheless, the uranyl ion could form non-complexible species such as $UO_2(CO_3)_3^{4-}$, $(UO_2)_2CO_3(OH)_3^-$ and $UO_2(OH)_3^-$ etc. in basis conditions (pH > 6), which leaded to the decrease of adsorption capability. Therefore, the maximum adsorption capacity of the material could be reached at pH 6.0.

Effect of contact time and adsorption kinetics

The effect of contact time on the adsorption capacity of uranium(VI) by MNPs@PAO at pH 6.0 and 298.15 K was tested. As shown in Fig. 9, the amount of uranium(VI) adsorbed on MNPs@PAO increased quickly in the first 4 h, increased slowly after that and reached equilibrium after 8 h. In order to study the kinetic mechanism of the adsorption process, the adsorption experimental data were simulated with the pseudo-first-order and pseudo-second-order models.The pseudo-first-order equation is as follows:

$$\ln(q_e - q_t) = \ln q_e - k_1 t \qquad (3)$$

The pseudo-second-order equation is as follows:

$$\frac{t}{q_t} = \frac{1}{k_2 q_e^2} + \frac{1}{q_e} t \qquad (4)$$

where the q_e and q_t are the adsorption capacities of U(VI) (mg/g) at equilibrium time and time t (h), respectively. The k_1 (h^{-1}) and k_2 (g mg^{-1} h^{-1}) are the rate constants of the pseudo-first-order and pseudo-second-order models, respectively.

Results of the linear regressions of the two models are shown in Fig. 10, and the calculated kinetic parameters are listed in Table 1. The correlation coefficient (R^2) value was 0.999 for the pseudo-second-order model, and the correlation coefficient value was 0.978 for the pseudo-first-order models. In addition, it is also found that the equilibrium adsorption capacity (q_e) calculated from the pseudo-second-order model (q_e (cal) = 176.37 mg/g) was in better agreement with the experimental data (q_e (exp) = 165.8 mg/g) in comparison with the pseudo-first-order model (q_e (cal) = 114.05 mg/g). These results suggest that the U(VI) adsorption process could be described well with the pseudo-second-order model, that the rate limiting step was the chemical adsorption, and that the adsorption process was dependent on the number of surface functional groups on the MNPs@PAO and the amount of the U(VI) ions existing in solutions [60, 61].

Effect of initial uranium concentrations and adsorption isotherm

Figure 11 shows the effect of initial uranium concentrations on the adsorption of uranium(VI) by MNPs@PAO. The equilibrium adsorption capacity of MNPs@PAO was increased with initial uranium concentration from 40 to 200 mg/L. The reason for this was probably that the
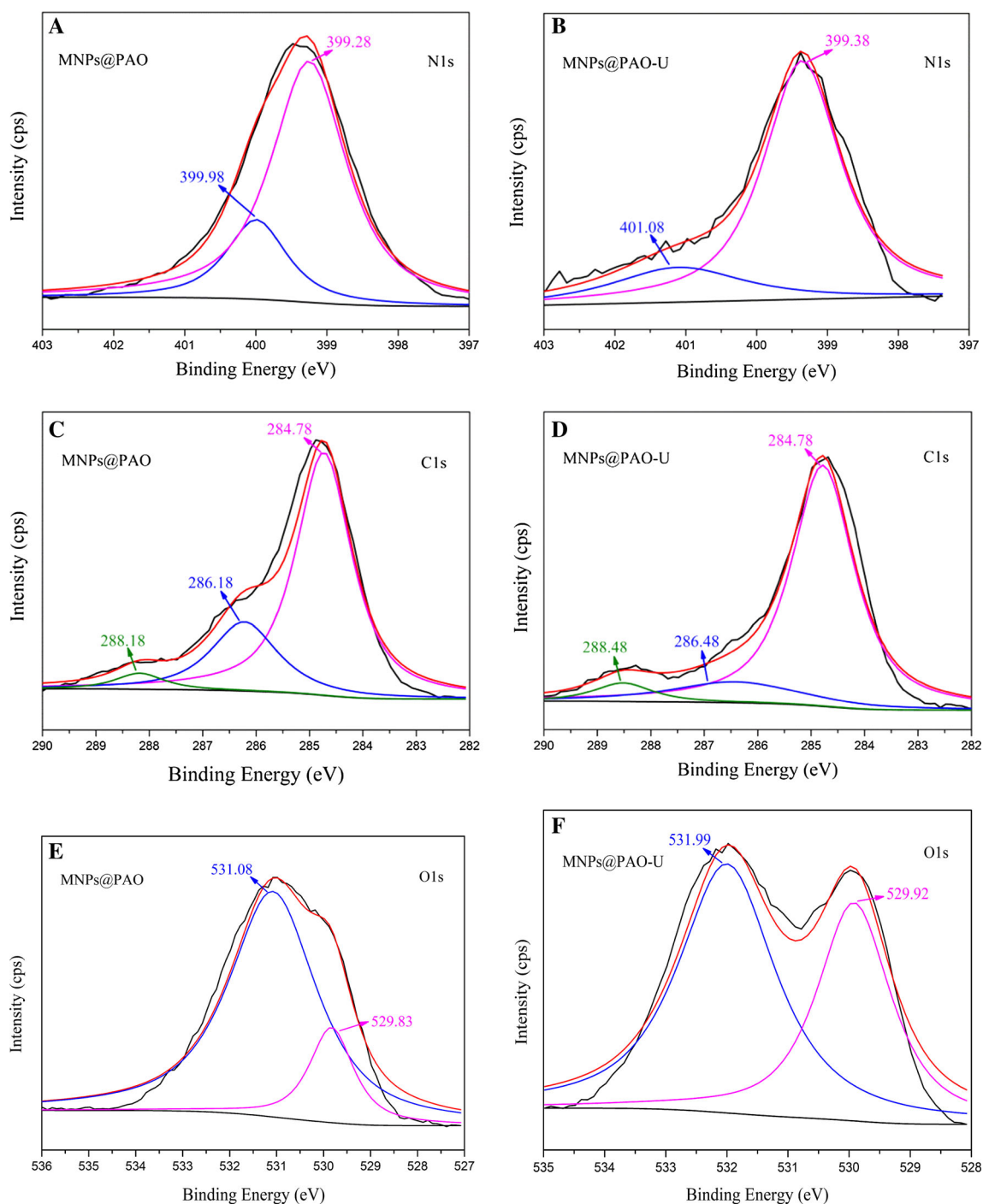
Fig. 6 XPS spectra of N1s for **a** MNPs@PAO, **b** MNPs@PAO-U and XPS spectra of C1s for **c** MNPs@PAO, **d** MNPs@PAO-U and XPS spectra of O1s for **e** MNPs@PAO, **f** MNPs@PAO-U

interaction between the uranyl ions and the adsorbent could be enhanced with the increasing initial uranium concentration. The similar phenomenon was also reported in the previous literatures [62].

The experimental data were simulated by Langmuir and Freundlich models to obtain the maximum adsorption amounts (q_m), and these two models were given below:

Langmuir model:

$$\frac{C_e}{q_e} = \frac{1}{q_m b_L} + \frac{1}{q_m} C_e \tag{5}$$

Freundlich model:

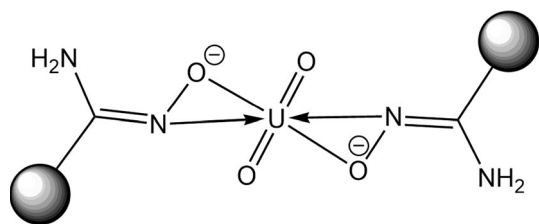$$\ln q_e = \ln K_F + \frac{1}{n_F} \ln C_e \tag{6}$$

Fig. 7 Possible $\eta 2$ chelating mechanism of U(VI) adsorption on MNPs@PAO
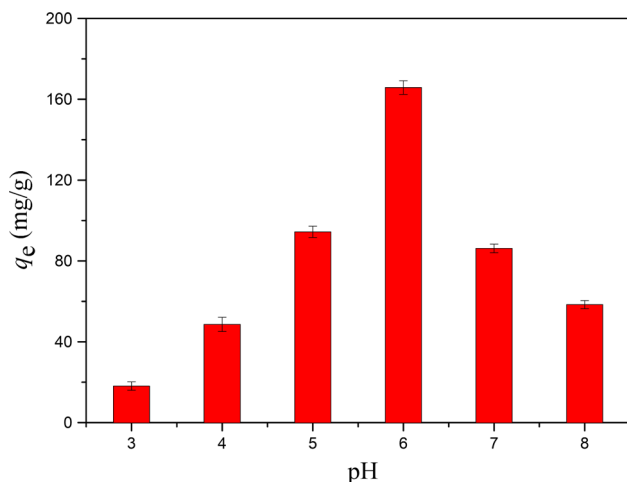

Fig. 8 Effect of pH on the U(VI) adsorption by MNPs@PAO ($m = 10$ mg, $V = 20$ mL, $C_o = 100$ mg/L, $T = 298.15$ K, $t = 20$ h)
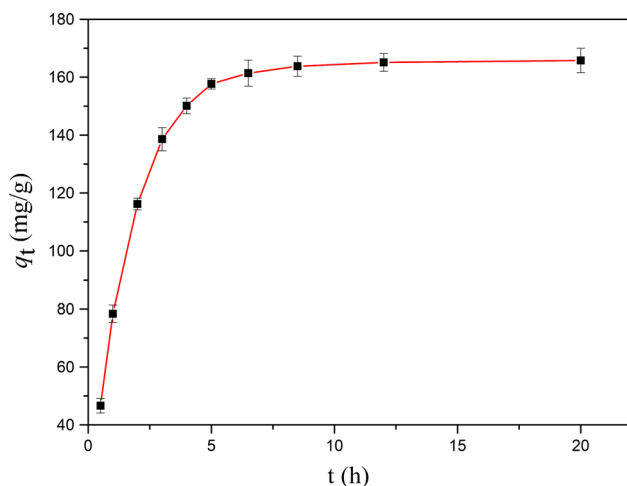

Fig. 9 Effect of contact time on the U(VI) adsorption by MNPs@PAO ($m = 10$ mg, $V = 20$ mL, $C_o = 100$ mg/L, pH 6.0, $T = 298.15$ K)

where C_e is the equilibrium concentration of U(VI) (mg/L). q_e is the amount of U(VI) adsorbed at equilibrium (mg/g). q_m and b_L are Langmuir constants related to maximum adsorption capacity and adsorption energy, respectively. K_F and n_F are Freundlich constants related to adsorption capacity and adsorption intensity, respectively.

Results of the linear regressions of the two models are shown in Fig. 12, and the calculated parameters of the Langmuir and Freundlich isotherms are listed in Table 2. Obviously, the Langmuir model ($R^2 = 0.999$) was found to fit the experimental results better than the Freundlich model ($R^2 = 0.904$) in terms of the correlation coefficient (R^2), and the maximum uranium (VI) adsorption capacity (q_m) of MNPs@PAO was calculated to be 216.45 mg/g. The results show that U(VI) adsorption onto MNPs@PAO is primarily a monolayer process rather than a multilayer one. In addition, the essential characteristics of the Langmuir isotherm can be explained in terms of separation factor R_L [63], which is defined by the following equation:

$$R_L = \frac{1}{1 + b_L C_o} \tag{7}$$

where b_L is Langmuir constant, and C_0 is the initial uranium concentration.

The values of R_L (Table 3) indicate that the adsorption of U(VI) by MNPs@PAO was favourable ($0 < R_L < 1$), and the adsorption was promoted at lower U(VI) concentration since the value of R_L was increased with the decrease of the U(VI) concentration [25, 63].

Effect of temperature and adsorption thermodynamics

In order to understand the mechanism of adsorption process, the effect of temperature on the adsorption of uranium(VI) was investigated. The results are shown in Fig. 13. The value of adsorption capacity of uranium(VI) was increased with the increasing temperature, which indicates that high temperature was more beneficial for the U(VI) adsorption than low temperature. It can be observed that the velocity of molecular movement was increased with the increasing temperature.

The thermodynamic parameters for adsorption of U(VI) onto MNPs@PAO were calculated using the Van't Hoff equation which is as follows:

$$\ln K_d = \frac{\Delta S^0}{R} - \frac{\Delta H^0}{RT} \tag{8}$$

where K_d is the distribution coefficient (mL/g), ΔS^0 is the standard entropy (J mol^{-1} K^{-1}), ΔH^0 is the standard enthalpy (kJ mol^{-1}), T is the reaction temperature (K), and R is the gas constant (8.314 J mol^{-1} K^{-1}).

The calculated thermodynamic parameters are listed in Tables 4 and 5. The results of the linear regressions of the equation were shown in Fig. 13b. The value of ΔH^0 is 35.06 kJ mol^{-1}, which indicates that the adsorption was endothermic, and the positive value of ΔS^0 ($\Delta S^0 = 136.11$ J/mol K) reveals that the adsorption was favorable and the randomness increased during the adsorption process.
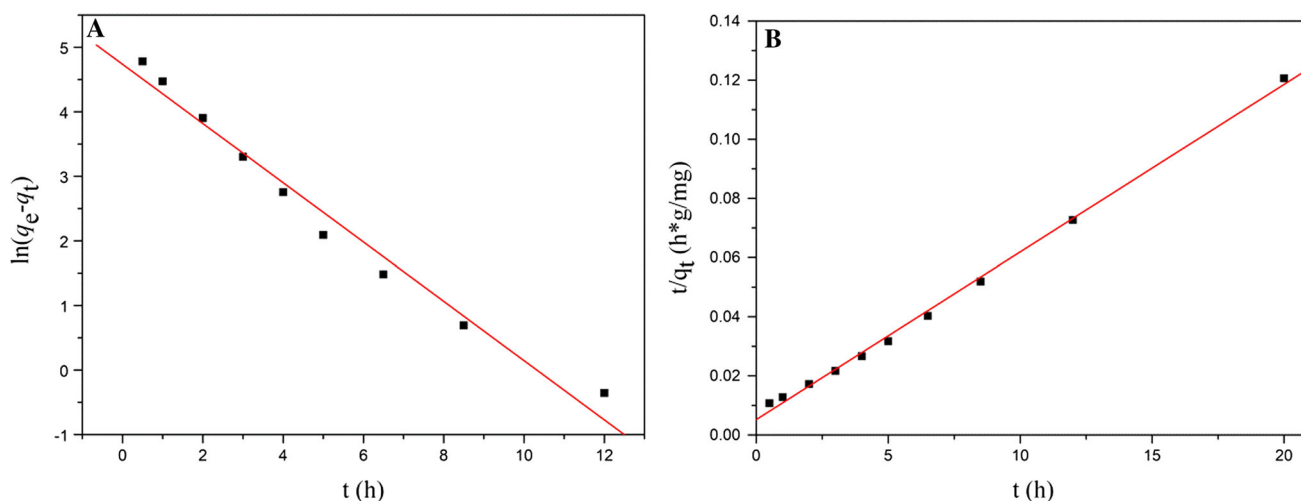
Fig. 10 Pseudo-first-order **a** and pseudo-second-order **b** plots for the adsorption of uranium(VI) by MNPs@PAO

Table 1 Kinetic parameters of U(VI) adsorption on MNPs@PAO

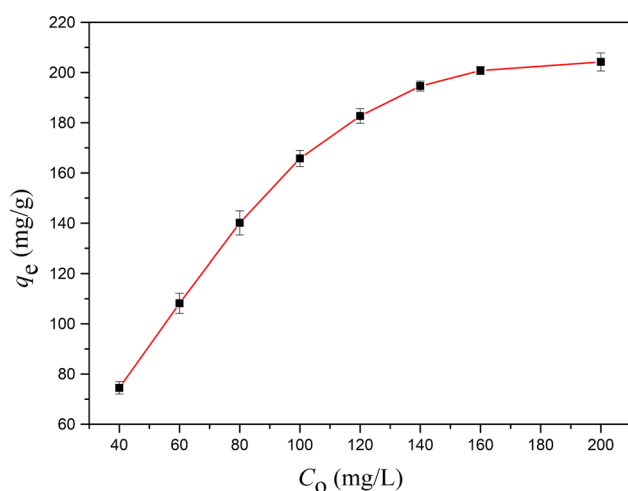| Q_e (exp) (mg/g)	Pseudo-first-order kinetics			Pseudo-second-order kinetics		
	K_1 (h^{-1})	q_e (cal) (mg/g)	R^2	K_2 (g mg^{-1} h^{-1})	Q_e (cal) (mg/g)	R^2
165.8	0.459	114.05	0.978	0.0058	176.37	0.999

Fig. 11 Effect of initial uranium concentrations on the U(VI) adsorption by MNPs@PAO ($m = 10$ mg, $V = 20$ mL, pH 6.0, $T = 298.15$ K, $t = 20$ h)

The standard Gibbs free energy (ΔG^0) values were calculated using the following equation:

$$\Delta G^0 = \Delta H^0 - T\Delta S^0 \tag{9}$$

The calculated values of ΔG^0 are listed in Table 5. As shown in the table, the values of ΔG^0 was declined with increasing temperature of solution from 298.15 K to 323.15 K, which indicates the adsorption process of uranium(VI) by MNPs@PAO was spontaneous and high temperature improved its adsorption property.

Effect of coexisting ions

Selectivity is an important index for performance evaluation of an adsorbent. The effect of coexisting metal ions, including Ca(II), Mn(II), Mg(II), Cd(II), Zn(II) and Co(II), on the adsorption of uranium by MNPs@PAO was investigated to evaluate the adsorption selectivity for uranium by MNPs@PAO. The selectivity coefficient ($S_{U/M}$) for U(VI) was determined using following formula [64]:

$$S_{U/M} = \frac{K_d^U}{K_d^M} \tag{10}$$

where K_d^U and K_d^M were distribution coefficients of MNPs@PAO for uranium(VI) and other coexisting ions, respectively.

The results are shown in Fig. 14 and listed in Table 6. It can be seen that q_e and K_d of MNPs@PAO for uranium(VI) were remarkably larger than those for the coexisting ions, which indicates that the adsorbent possessed a desirable selectivity for U(VI) over a range of coexisting metal ions. The reason for this was probably that the amidoxime-based ligands were grafted on the surface of nanoparticles through surface-initiated RAFT polymerization. Amidoxime, as an excellent amphoteric functional group containing both acidic (–OH) and basic (–NH$_2$) sites, has shown a strong tendency to form a stable chelate which can complex with the uranyl ion (UO$_2^{2+}$). The lone pairs of electrons in the amino nitrogen and oxime oxygen can be
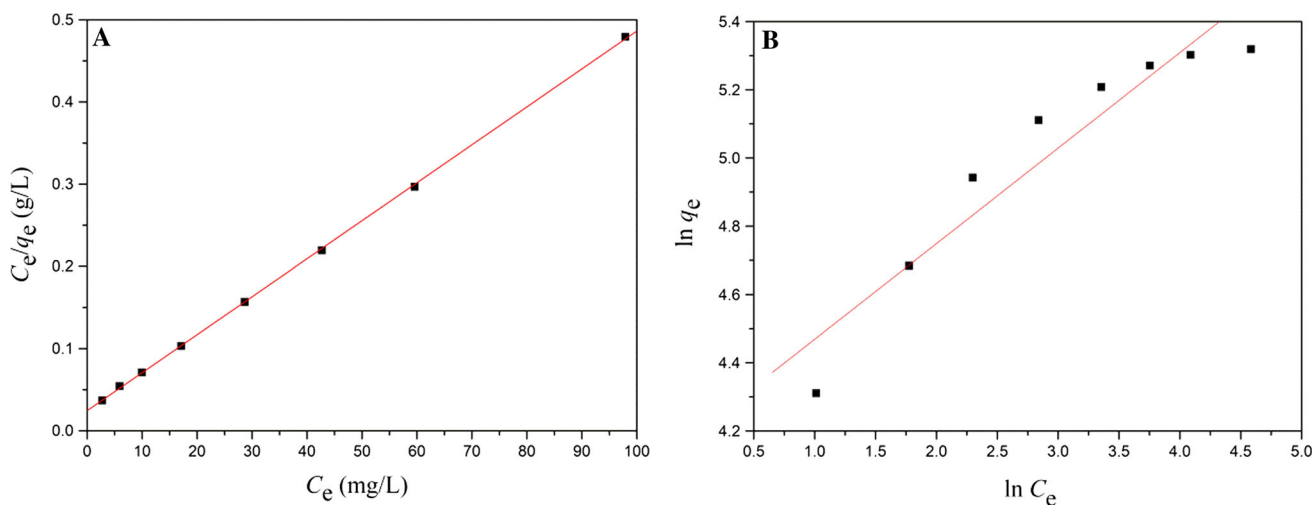
Fig. 12 Langmuir (**a**) and Freundlich (**b**) for the adsorption of uranium (VI) by MNPs@PAO

Table 2 Parameters of the Langmuir and Freundlich isotherms for the adsorption of uranium (VI)

Langmuir isotherm			Freundlich isotherm		
B_L	Q_m (mg/g)	R^2	K_F	N_F	R^2
0.1886	216.45	0.999	13.21	2.03	0.904

Table 4 Thermodynamic parameters for adsorption of U(VI) onto MNPs@PAO

ΔH^0 (kJ/mol)	ΔS^0 (J/mol·K)	R^2
35.06	136.11	0.991

donated to the UO_2^{2+} center to form a stable chelate [15, 65, 66]. Therefore, the amidoxime-based ligands grafted on the surface of nanoparticles can significantly improve the adsorption selectivity of adsorbent for the uranyl ions in aqueous solution.

Table 3 The Langmuir separation factor R_L

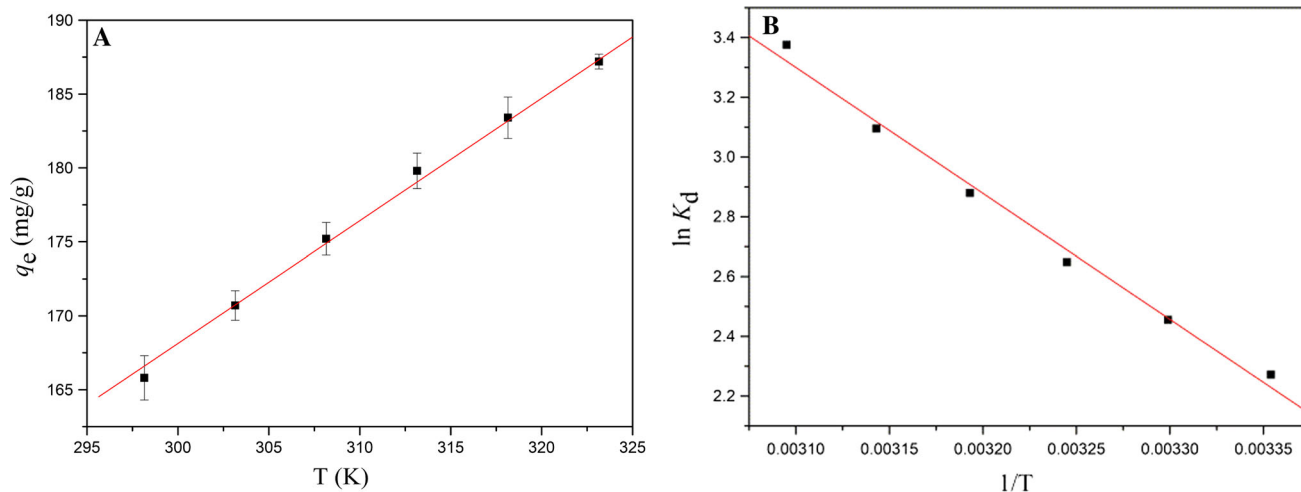| U(VI) initial concentration (mg/L)	40	60	80	100	120	140	160	200
R_L	0.117	0.081	0.062	0.050	0.042	0.036	0.027	0.026

Fig. 13 Effect of temperature on the U(VI) adsorption by MNPs@PAO (**a**) and the relationship curve between $\ln K_d$ and $1/T$ (**b**) ($m = 10$ mg, $V = 20$ mL, pH 6.0, $t = 8$ h)

Table 5 ΔG^0 for adsorption of U (VI) onto MNPs@PAO at different temperatures

T (K)	298.15	303.15	308.15	313.15	318.15	323.15
ΔG^0 (kJ/mol)	− 5.52	− 6.20	− 6.88	− 7.56	− 8.24	− 8.92
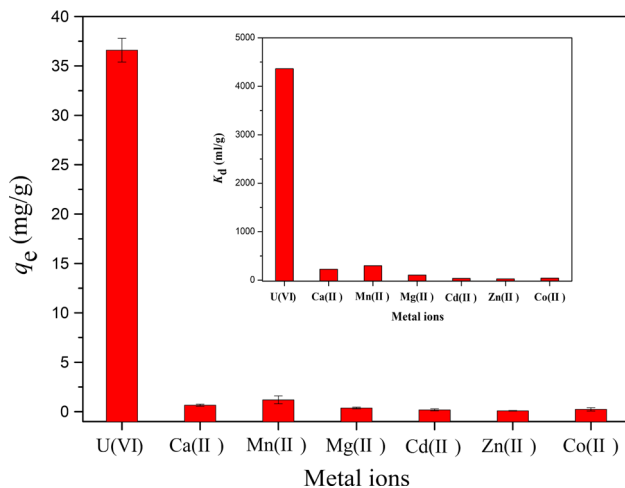
Fig. 14 Selective adsorption of uranium by MNPs@PAO ($m = 10$ mg, $V = 20$ mL, $C_o \approx 0.1$ mmol/L for all metal ions, pH 6.0, $T = 298.15$ K, $t = 8$ h)

Table 6 Distribution coefficients (K_d) and selectivity coefficients (S_U) of MNPs@PAO

Ions	K_d (mL/g)	S_U
U(VI)	4362.86	–
Ca(II)	226.05	19.30
Mn(II)	298.15	14.63
Mg(II)	102.78	42.45
Cd(II)	36.78	118.62
Zn(II)	27.19	160.46
Co(II)	40.85	106.80

Fig. 15 Recycling of MNPs@PAO in the uranium adsorption

Desorption and regeneration studies

Regeneration of an adsorbent is important for evaluating its economic efficiency in application potential. In this work, the MNPs@PAO loaded with uranium(VI) was eluted with 0.1 M HCl solution after the adsorption. The adsorption and desorption experiments were cycled five times. Figure 15 shows that the adsorption capacity of MNPs@PAO for U(VI) only decreased 15.25% after five successive adsorption/desorption cycles, indicating that the adsorbent had good reversibility.

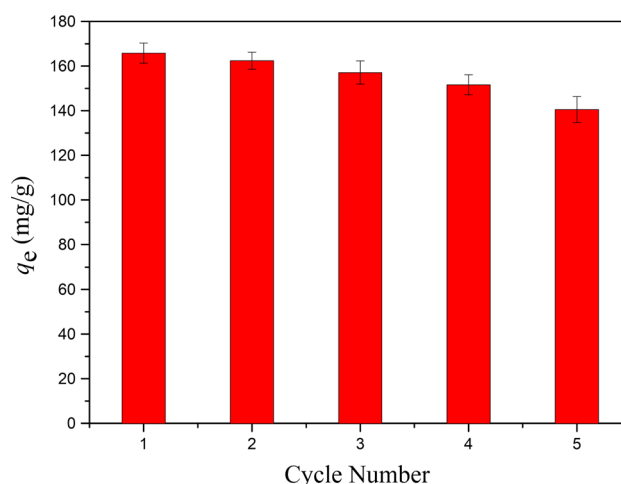## Comparison of uranium(VI) adsorption capacity with other adsorbents

Table 7 presents the comparison of uranium(VI) adsorption capacity with other adsorbents. As shown in the table, the maximum adsorption capacity of uranium on MNPs@PAO reaches equal to 165.8 mg/g, which is higher than that on other adsorbents. Thus, the MNPs@PAO adsorbent is suitable for the adsorption of uranium (VI).

Conclusions

In conclusion, a novel core–shell magnetic nanocomposite MNPs@PAO was successfully synthesized by surface-initiated RAFT polymerization. The adsorption experiment results showed that it had high adsorption capacity and good selectivity for uranium(VI) under optimized conditions due to its large surface area and its strong chelation with amidoxime ligands. The studies on the adsorption kinetic and isotherm revealed that the adsorption process fitted well with pseudo-second order kinetic model and Langmuir adsorption isotherm model, indicating that the chemical adsorption was the controlling step and the uranium ions were adsorbed on the homogeneous surface in monolayer. The thermodynamic parameters implied that the adsorption process of uranium(VI) by MNPs@PAO was endothermic and spontaneous. Moreover, the adsorbent could be regenerated efficiently after five cycles and still had high adsorption capacity. Therefore, this work provides a useful method for preparing core–shell magnetic nanocomposite by surface-initiated RAFT polymerization for the separation of uranium or other heavy metal ions from aqueous solutions.

Table 7 Comparison of adsorption capacities for uranium(VI) of various adsorbents

Adsorbent	Experimental conditions	Q_m (mg/g)	References
SII-PNF	298.15 K, 15 h, pH 8.0	133.3	[39]
Fe$_3$O$_4$@PDA@PAO	298 K, 5 h pH 5.0	162.5	[23]
P-Fe-CMK-3	298.15 K, 5 min, pH 4.0	150	[34]
POMN	298.15 K, 5 min, pH 8.0	141.4	[67]
TMP-g-AO	298 K, 72 h, pH 8.2	35.4	[28]
CPP	298 K, 3 h, pH 8	146.6	[21]
MNPs@PAO	298.15 K, 8 h, pH 6.0	165.8	This work

References

1. Zolfaghari G, Esmaili-Sari A, Anbia M, Younesi H, Amirmahmoodi S, Ghafari-Nazari A (2011) Taguchi optimization approach for Pb(II) and Hg(II) removal from aqueous solutions using modified mesoporous carbon. J Hazard Mater 192:1046–1055

2. Rao TP, Metilda P, Gladis JM (2006) Preconcentration techniques for uranium(VI) and thorium(IV) prior to analytical determination-an overview. Talanta 68:1047–1064

3. Raju CSK, Subramanian MSA (2007) Sequential separation of lanthanides, thorium and uranium using novel solid phase extraction method from high acidic nuclear wastes. J Hazard Mater 145:315–322

4. Mellah A, Chegrouche S, Barkat M (2006) The removal of uranium(VI) from aqueous solutions onto activated carbon: kinetic and thermodynamic investigations. J Colloid Interface Sci 296:434–441

5. Schmitt P, Beer PD, Drew MGB, Sheen PD (1998) Uranyl binding by a novel bis-calix[4]arene receptor. Tetrahedron Lett 39:6383–6386

6. Wang JQ, Li X, Li SP, Zhong H (2011) Studies on preparation of methotrexatum/layered double hydroxides compounds by coprecipitation method in ethanol-water medium. Acta Chim Sinica 69:137–144

7. Favre-Réguillon A, Lebuzit G, Murat D, Foos J, Mansour C, Draye M (2008) Selective removal of dissolved uranium in drinking water by nanofiltration. Water Res 42:1160–1166

8. Liu Q, Zhu J, Tan L, Jing X, Liu J, Song D, Zhang H, Li R, Emelchenko G, Wang J (2016) Polypyrrole/cobalt ferrite/multiwalled carbon nanotubes as an adsorbent for removing uranium ions from aqueous solutions. Dalton Trans 45:9166–9173

9. Djedidi Z, Bouda M, Souissi MA, Cheikh RB, Mercier G, Tyagi RD, Blais JF (2009) Metals removal from soil, fly ash and sewage sludge leachates by precipitation and dewatering properties of the generated sludge. J Hazard Mater 172:1372–1382

10. Gorden AEV, Xu J, Raymond KN (2003) Rational design of sequestering agents for plutonium and other actinides. Chem Rev 103:4207–4282

11. Sather AC, Berryman OB, Rebek J (2010) Selective recognition and extraction of the uranyl ion. J Am Chem Soc 132:13572–13574

12. Beer S, Berryman OB, Ajami D (2010) Encapsulation of the uranyl dication. Chem Sci 1:43–47

13. Mishra S, Dwivedi J, Kumar A, Sankararamakrishnan N (2015) Studies on salophen anchored micro/meso porous activated carbon fibres for the removal and recovery of uranium. RSC Adv 5:33023–33036

14. Zhao Y, Wang X, Li J, Wang X (2015) Amidoxime functionalization of mesoporous silica and its high removal of U(VI). Polym Chem 6:5376–5384

15. Gunathilake C, Górka J, Dai S, Jaroniec M (2015) Amidoxime-modified mesoporous silica for uranium adsorption under seawater conditions. J Mater Chem A 3:11650–11659

16. Florek J, Giret S, Juere E, Lariviere D, Kleitz F (2016) Functionalization of mesoporous materials for lanthanide and actinide extraction. Dalton Trans 45:14832–14854

17. Li R, Che R, Liu Q, Su S, Li Z, Zhang H, Liu J, Liu L, Wang J (2017) Hierarchically structured layered-double-hydroxides derived by ZIF-67 for uranium recovery from simulated seawater. J Hazard Mater 338:167–176

18. Li B, Ma L, Tian Y, Yang X, Li J, Bai C, Yang X, Zhang S, Li S, Jin Y (2014) A catechol-like phenolic ligand-functionalized hydrothermal carbon: one-pot synthesis, characterization and sorption behavior toward uranium. J Hazard Mater 271:41–49

19. Zhang S, Zhao X, Li B, Bai C, Li Y, Wang L, Wen R, Zhang M, Ma L, Li S (2016) "Stereoscopic" 2D super-microporous phosphazene-based covalent organic framework: design, synthesis and selective sorption towards uranium at high acidic condition. J Hazard Mater 314:95–104

20. Li J, Yang X, Bai C, Tian Y, Li B, Zhang S, Yang X, Ding S, Xia C, Tan X, Ma L, Li S (2015) A novel benzimidazole-functionalized 2-D COF material: synthesis and application as a selective solid-phase extractant for separation of uranium. J Colloid Interface Sci 437:211–218

21. Brown S, Chatterjee S, Li M, Yue Y, Tsouris C, Janke CJ, Saito T, Dai S (2016) Uranium adsorbent fibers prepared by atom-transfer radical polymerization from chlorinated polypropylene and polyethylene trunk fibers. Ind Eng Chem Res 55:4130–4138

22. Brown S, Yue Y, Kuo L-J, Mehio N, Li M, Gill GA, Tsouris C, Mayes RT, Saito T, Dai S (2016) Uranium adsorbent fibers prepared by atom-transfer radical polymerization (ATRP) from poly(vinyl chloride)-co-chlorinated poly(vinyl chloride) (PVC-co-CPVC) fiber. Ind Eng Chem Res 55:4139–4148

23. Zhu J, Liu Q, Li Z, Liu J, Zhang H, Li R, Wang J, Emelchenko GA (2017) Recovery of uranium (VI) from aqueous solutions by the modified honeycomb-like porous carbon material. Dalton Trans 46:420–429

24. Wu F, Pu N, Ye G, Sun T, Wang Z, Song Y, Wang W, Huo X, Lu Y, Chen J (2017) Performance and mechanism of uranium adsorption from seawater to poly(dopamine)-inspired sorbents. Environ Sci Technol 51:4606–4614

25. Dong Y, Dong Z, Zhang Z, Liu Y, Cheng W, Miao H, He X, Xu Y (2017) POM constructed from super-sodalite cage with extra-large 24-membered channels: effective sorbent for uranium adsorption. ACS Appl Mater Interfaces 9:22088–22092

26. Li Y, Wang L, Li B, Zhang M, Wen R, Guo X, Li X, Zhang J, Li S, Ma L (2016) Pore-free matrix with cooperative chelating of hyperbranched ligands for high-performance separation of uranium. ACS Appl Mater Interfaces 8:28853–28861

27. Yang Y, Wang J, Wu F, Ye G, Yi R, Lu Y, Chen J (2016) Surface-initiated SET-LRP mediated by mussel-inspired polydopamine chemistry for controlled building novel core-shell magnetic nanoparticles for highly-efficient uranium enrichment. Polym Chem 7:2427–2435

28. Zeng J, Zhang H, Sui Y, Hu N, Ding D, Wang F, Xue J, Wang Y (2017) New amidoxime based material TMP-g-AO for uranium adsorption under seawater conditions. Ind Eng Chem Res 56:5021–5032

29. Hu B, Ye F, Ren X, Zhao D, Sheng G, Li H, Ma J, Wang X, Huang Y (2016) X-ray absorption fine structure study of enhanced sequestration of U(VI) and Se(IV) by montmorillonite decorated with zero-valent iron nanoparticles. Environ Sci Nano 3:1460–1472

30. Hu B, Hu Q, Xu D, Chen C (2017) The adsorption of U(VI) on carbonaceous nanofibers: a combined batch, EXAFS and modeling techniques. Sep Purif Technol 175:140–146

31. Linghu W, Sun Y, Yang H, Chang K, Ma J, Huang Y, Dong W, Alsaedi A, Hayat T (2017) Sorption of U(VI) on magnetic sepiolite investigated by batch and XANES techniques. J Radioanal Nucl Chem 314:1825–1832

32. Dong L, Yang J, Mou Y, Sheng G, Wang L, Linghu W, Asiri AM, Alamry KA (2017) Effect of various environmental factors on the adsorption of U(VI) onto biochar derived from rice straw. J Radioanal Nucl Chem 314:377–386

33. Linghu W, Yang H, Sun Y, Sheng G, Huang Y (2017) One-pot synthesis of LDH/GO composites as highly effective adsorbents for decontamination of U(VI). ACS Sustain Chem Eng 5:5608–5616

34. Husnain SM, Um W, Chang Y-Y, Chang Y-S (2017) Recyclable superparamagnetic adsorbent based on mesoporous carbon for sequestration of radioactive Cesium. Chem Eng J 308:798–808

35. Mohapatra S, Rout SR, Das RK, Nayak S, Ghosh SK (2016) Highly hydrophilic luminescent magnetic mesoporous carbon nanospheres for controlled release of anticancer drug and multimodal imaging. Langmuir 32:1611–1620

36. Wang J, Zhou H, Zhuang J, Liu Q (2015) Magnetic γ-Fe$_2$O$_3$, Fe$_3$O$_4$, and Fe nanoparticles confined within ordered mesoporous carbons as efficient microwave absorbers. Phys Chem Chem Phys 17:3802–3812

37. Cheng M, Wang Z, Lv Q, Li C, Sun S, Hu S (2018) Preparation of amino-functionalized Fe$_3$O$_4$@mSiO$_2$ core-shell magnetic nanoparticles and their application for aqueous Fe^{3+} removal. J Hazard Mater 341:198–206

38. Min X, Yang W, Hui Y-F, Gao C-Y, Dang S, Sun Z-M (2017) Fe$_3$O$_4$@ZIF-8: a magnetic nanocomposite for highly efficient UO$_2^{2+}$ adsorption and selective UO$_2^{2+}$/Ln^{3+} separation. Chem Commun 53:4199–4202

39. Zhang L, Yang S, Qian J, Hua D (2017) Surface ion-imprinted polypropylene nonwoven fabric for potential uranium seawater extraction with high selectivity over vanadium. Ind Eng Chem Res 56:1860–1867

40. Horzum N, Shahwan T, Parlak O, Demir MM (2012) Synthesis of amidoximated polyacrylonitrile fibers and its application for sorption of aqueous uranyl ions under continuous flow. Chem Eng J 213:41–49

41. Barber PS, Kelley SP, Griggs CS, Wallace S, Rogers RD (2014) Surface modification of ionic liquid-spun chitin fibers for the extraction of uranium from seawater: seeking the strength of chitin and the chemical functionality of chitosan. Green Chem 16:1828–1836

42. Gao Q, Hu J, Li R, Xing Z, Xu L, Wang M, Guo X, Wu G (2016) Radiation synthesis of a new amidoximated UHMWPE fibrous adsorbent with high adsorption selectivity for uranium over vanadium in simulated seawater. Radiat Phys Chem 122:1–8

43. Oyola Y, Dai S (2016) High surface-area amidoxime-based polymer fibers co-grafted with various acid monomers yielding increased adsorption capacity for the extraction of uranium from seawater. Dalton Trans 45:8824–8834

44. Wilczewska AZ, Markiewicz KH (2014) Surface-initiated RAFT/MADIX polymerization on xanthate-coated iron oxide nanoparticles. Macromol Chem Phys 215:190–197

45. Moorthy MS, Oh Y, Bharathiraja S, Manivasagan P, Rajarathinam T, Jang B, VyPhan TT, Jang H, Oh J (2016) Synthesis of amine-polyglycidol functionalized Fe$_3$O$_4$@SiO$_2$ nanocomposites for magnetic hyperthermia, pH-responsive drug delivery, and bioimaging applications. RSC Adv 6:110444–110453

46. Liu X, Liu H, Ma H, Cao C, Yu M, Wang Z, Deng B, Wang M, Li J (2012) Adsorption of the uranyl ions on an amidoxime-based polyethylene nonwoven fabric prepared by preirradiation-induced emulsion graft polymerization. Ind Eng Chem Res 51:15089–15095

47. Das S, Tsouris C, Zhang C, Kim J, Brown S, Oyola Y, Janke CJ, Mayes RT, Kuo LJ, Wood JR (2016) Enhancing uranium uptake by amidoxime adsorbent in seawater: an investigation for optimum alkaline conditioning parameters. Ind Eng Chem Res 55:4294–4302

48. Hao Z, Wang D, Chen H, Sun J, Xu Y (2014) Sweet potato starch residue as starting material to prepare polyacrylonitrile adsorbent via SI-SET-LRP. J Agric Food Chem 62:1765–1770

49. Lu X, He SN, Zhang DX, Reda AT, Liu C, Feng J, Yang Z (2016) Synthesis and characterization of amidoxime modified calix[8]-arene for adsorption of U(VI) in low concentration uranium solutions. RSC Adv 6:101087–101097

50. Shao DD, Wang XX, Wang XL, Hu S, Hayat T, Alsaedi A, Li JX, Wang SH, Hu J, Wang XK (2016) Zero valent iron/poly(amidoxime) adsorbent for the separation and reduction of U(VI). RSC Adv 6:52076–52081

51. Husnain SM, Kim H, Um W, Chang Y-Y, Chang Y-S (2017) Superparamagnetic adsorbent based on phosphonate grafted mesoporous carbon for uranium removal. Ind Eng Chem Res 56:9821–9830

52. Zhao Y, Li J, Zhang S, Wang X (2014) Amidoxime-functionalized magnetic mesoporous silica for selective sorption of U(VI). RSC Adv 4:32710–32717

53. Chi FT, Hu S, Xiong J, Wang XL (2013) Adsorption behavior of uranium on polyvinyl alcohol-g-amidoxime: physicochemical properties, kinetic and thermodynamic aspects. Sci China Chem 56:1495–1503

54. Manos MJ, Kanatzidis MG (2012) Layered metal sulfides capture uranium from seawater. J Am Chem Soc 134:16441–16446

55. Tian Y, Fu J, Zhang Y, Cao K, Bai C, Wang D, Li S, Xue Y, Ma L, Zheng C (2015) Ligand-exchange mechanism: new insight into solid-phase extraction of uranium based on a combined experimental and theoretical study. Phys Chem Chem Phys 17:7214–7223

56. Li B, Bai C, Zhang S, Zhao X, Li Y, Wang L, Ding K, Shu X, Li S, Ma L (2015) An adaptive supramolecular organic framework for highly efficient separation of uranium via an in situ induced fit mechanism. J Mater Chem A 3:23788–23798

57. Vukovic S, Watson LA, Kang SO, Custelcean R, Hay BP (2012) How amidoximate binds the uranyl cation. Inorg Chem 51:3855–3859

58. Parker BF, Zhang Z, Rao L, Arnold J (2018) An overview and recent progress in the chemistry of uranium extraction from seawater. Dalton Trans 47:639–644

59. Li S, Bai H, Wang J, Jing X, Liu Q, Zhang M, Chen R, Liu L, Jiao C (2012) In situ grown of nano-hydroxyapatite on magnetic CaAl-layered double hydroxides and its application in uranium removal. Chem Eng J 193:372–380

60. Ho Y-S (2006) Review of second-order models for adsorption systems. J Hazard Mater 136:681–689

61. Tan X, Ren X, Li J, Wang X (2013) Theoretical investigation of uranyl ion adsorption on hydroxylated γ-Al_2O_3 surfaces. RSC Adv 3:19551–19559

62. Chen SP, Hong JX, Yang HX, Yang JZ (2013) Adsorption of uranium (VI) from aqueous solution using a novel graphene oxide- activated carbon felt composite. J Environ Radioact 126:253–258

63. Zhao Y, Liu C, Feng M, Chen Z, Li S, Tian G, Wang L, Huang J, Li S (2010) Solid phase extraction of uranium(VI) onto benzoylthiourea-anchored activated carbon. J Hazard Mater 176:119–124

64. Preetha CR, Gladis JM, Rao TP, Venkateswaran G (2006) Removal of toxic uranium from synthetic nuclear power reactor effluents using uranyl ion imprinted polymer particles. Environ Sci Technol 40:3070–3074

65. Lu X, Zhang D, Reda AT, Liu C, Yang Z, Guo S, Xiao S, Ouyang Y (2017) Synthesis of amidoxime-grafted activated carbon fibers for efficient recovery of uranium(VI) from aqueous solution. Ind Eng Chem Res 41:11936–11947

66. Kelley SP, Barber PS, Mullins PHK, Rogers RD (2014) Structural clues to UO_2^{2+}/VO^{2+} competition in seawater extraction using amidoxime-based extractants. Chem Commun 50:12504–12507

67. Xu M, Han X, Hua D (2017) Polyoxime-functionalized magnetic nanoparticles for uranium adsorption with high selectivity over vanadium. J Mater Chem A 5:12278–12284